The discovery of 64 luminous infrared galaxies in the LAMOST Complete Spectroscopic Survey of Pointing Area at the Southern Galactic Cap

Man I Lam[1,2], Hong Wu[1], Ming Yang[1], Yi-Nan Zhu[1], Jian-Rong Shi[1], Hao-Tong Zhang[1], A-Li Luo[1], Shi-Yin Shen[3], Yong Zhang[4], Yong-Hui Hou[4], Guang-Wei Li[1] and Yong-Heng Zhao[1]

[1] Key Laboratory of Optical Astronomy, National Astronomical Observatories, Chinese Academy of Sciences, Beijing 100012, China; *linminyi@nao.cas.cn*
[2] University of Chinese Academy of Sciences, Beijing 100049, China
[3] Key Laboratory for Research in Galaxies and Cosmology, Shanghai Astronomical Observatory, Chinese Academy of Sciences, Shanghai 200030, China
[4] Nanjing Institute of Astronomical Optics & Technology, National Astronomical Observatories, Chinese Academy of Sciences, Nanjing 210042, China

Abstract We report the discovery of 64 luminous infrared galaxies, based on new observations of 20 square degrees from the LAMOST Complete Spectroscopic Survey of Pointing Area at the Southern Galactic Cap and the WISE 22 μm catalog from the AllWISE Data Release. Half of them are classified as late-type spirals and the others are classified as peculiar/compact galaxies. The peculiar/compact galaxies tend to exhibit higher luminosities and lower stellar masses. We also separate AGNs from HII galaxies in a simple way by examining LAMOST spectra. Those cases show that host AGNs are easily distinguished from others in the mid-infrared color-color diagrams.

Key words: galaxies: statistic — galaxies: structure — galaxies: starburst — galaxies: spiral — galaxies: interactions — infrared: galaxies

1 INTRODUCTION

Our knowledge of the infrared (IR) universe achieved a breakthrough after the launch of the *Infrared Astronomical Satellite* (IRAS) in 1983 (Neugebauer et al. 1984; Soifer et al. 1987). New types of infrared objects with extremely high luminosity in the local universe were discovered, which were later named *Ultra-Luminous Infrared Galaxies* ($L_{\rm IR(8-1000\,\mu m)} \geqslant 10^{12} L_\odot$; ULIRGs) and *Luminous Infrared Galaxies* ($L_{\rm IR(8-1000\,\mu m)} \geqslant 10^{11} L_\odot$; LIRGs) (Sanders & Mirabel 1996). Although the number density of LIRGs/ULIRGs is quite low, they still make a significant contribution to the nearby infrared universe.

Multi-wavelength observations and analysis have indicated that they are dominated by circumnuclear dust heated from starbursts and active galactic nuclei (AGNs) (e.g. Wu et al. 1998b). Pioneering works showed that most ULIRGs can be classified as interacting or merging systems

(e.g. Zou et al. 1991; Sanders & Mirabel 1996), and may be the transitional stages from merging starbursts to classical optical AGNs (e.g. Surace et al. 1998). However, LIRGs seem to have some differences. Wu et al. (1998a,b) constructed a sample of very luminous LIRGs and found that, with increasing IR luminosities, the fraction of interaction/merging systems also increased. Ishida (2004) supported such results and pointed out that optical morphological types and other properties (e.g. molecular gas contents and mid-infrared colors) were closely related with IR luminosity. For galaxies with IR luminosity above $10^{11.5} L_\odot$, almost all of them were found in merging/interacting systems. Based on a large sample of LIRGs, which was cross-identified from SDSS DR 2 and IRAS (Cao et al. 2006), Wang et al. (2006) selected and analyzed the properties of a sub-sample of 159 LIRGs. Among them, $\sim 48\%$ of the sample galaxies were classified as interacting/merging systems, and the others were spiral or compact galaxies. The fraction of spiral galaxies in their sample increased in the redshift range from $z = 0.1$ to 1, which was consistent with the result presented by Melbourne et al. (2005). Afterward, Wang (2008) studied a sample with wider infrared luminosity ranges, which included both LIRGs and ULIRGs, and the previous result was still valid up to $z \lesssim 0.08$. However, Hung et al. (2014) found that the fraction of interacting/merging systems showed less evolution until $z \sim 1$. Therefore, the evolution of LIRGs is still controversial.

The new all-sky survey *Wide-field Infrared Survey Explorer* (WISE; Wright et al. 2010) mission provides a data set with unprecedented sensitivity and size. The mission simultaneously has surveyed images in four mid-infrared bands at wavelengths of 3.4 (W1), 4.6 (W2), 12 (W3) and 22 (W4) μm. The 5σ flux limited sample of point sources is better than 0.05, 0.1, 0.75 and 6 mJy, and the angular resolution is $6.1''$, $6.4''$, $6.5''$ and $12.0''$, respectively (Yan et al. 2013). Su et al. (2013) carefully selected and thoroughly studied a large sample of ULIRGs based on WISE and SDSS, and they found there was no evolutionary link between the ULIRGs with or without AGNs. Moreover, Eisenhardt et al. (2012) found a type of rare, hot, dust-obscured hyper-luminous infrared galaxy at high redshift by using WISE. However, LIRGs with relatively lower infrared luminosity in WISE have still not been studied in detail. With the better angular resolution and wide field provided by the WISE all sky survey and Large Sky Area Multi-Object Fiber Spectroscopic Telescope (LAMOST) extragalactic spectroscopic survey, we can re-analyze the morphologies and mechanisms of a sample of LIRGs.

LAMOST (Zhao et al. 2012), also called the Guo Shou Jing Telescope, is a Wang-Su Schmidt telescope with an effective aperture of 4 m. It has a $5°$ field of view that can use up to 4000 fibers in a single exposure. As one of the key science projects that is part of the LAMOST research program (Liu et al. 2015), the LAMOST Complete Spectroscopic Survey of Pointing Area (LCSSPA) at the Southern Galactic Cap (SGC), is designed to observe all magnitude-limited objects in two areas of 20 square degrees in regions near the SGC. The limiting magnitude of this survey is $r = 18.1$ mag (Yang et al. 2014 in preparation). At the end of 2013, observations of the first field were finished. In this paper, we only focus on the first field to identify LIRGs, and analyze their morphological types and properties.

In the following sections, data reduction and sample selection are presented in Section 2. The results and analysis are described in Section 3. The discussion and summary are presented in Section 4 and Section 5, respectively. We adopt a cosmology with constants of $\Omega_m = 0.3$, $\Omega_\Lambda = 0.7$ and $H_0 = 70$ km s^{-1} Mpc^{-1} throughout this work.

2 DATA AND SAMPLE SELECTION

2.1 LAMOST Data and Reduction

The resolution of LAMOST spectra is R ~ 1800, and the wavelength ranges from 3700 Å to 9100 Å (Fig. 1), which includes the blue channel from 3700 Å to 5900Å and the red channel from 5700 Å to 9100 Å (Cui et al. 2012; Zhao et al. 2012). The LCSSPA at SGC is designed to observed all sources (both stars and galaxies) in two selected fields of 20 deg^2 at the SGC with a limiting magnitude of
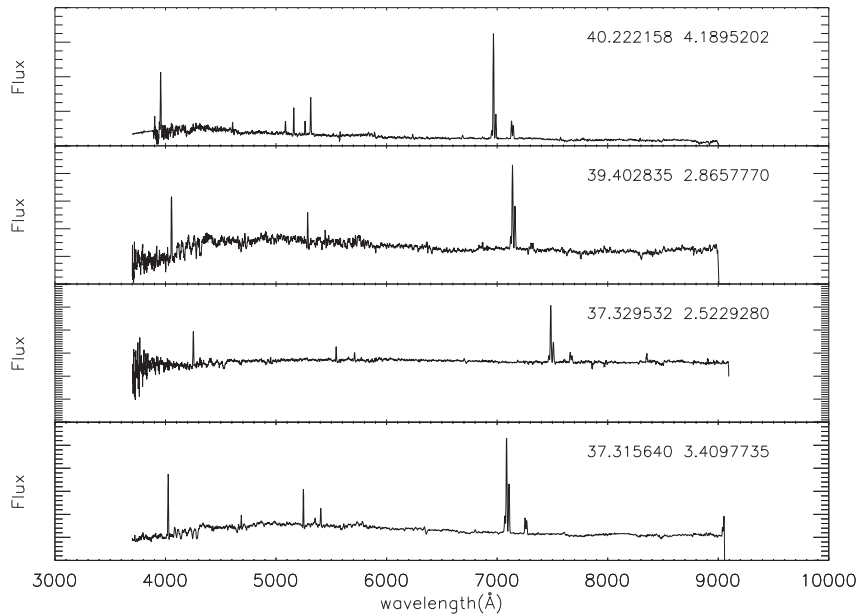
Fig. 1 Sample spectra of LIRGs selected from the LAMOST survey.

$r = 18.1$ mag. To test possible environmental effects, one region with high galactic number density and one region with low number density are selected and also included in the SGC u-band sky survey (SCUSS; Zhou et al., in preparation). The centers of the two fields are RA = 37.88 deg, Dec = 3.44 deg (hereafter Field A) and RA = 21.53 deg, Dec = −2.20 deg (hereafter Field B), which represent the low and high density fields, respectively.

Among all the selected targets in Field A, there are 2519 galaxies, 97% of which were successfully observed (for more details see Yang et al. 2014 in preparation).

The raw data are first reduced by the LAMOST two-dimensional and one-dimensional pipelines (Luo et al. 2012), which include bias subtraction, flat-field correction, cosmic-ray removal, spectral wavelength calibration, spectral transformation correction and sky subtraction. Due to the limitations of low signal-to-noise ratio (SNR) and sky subtraction of spectra, the redshift values of only one-third of the extragalactic objects were obtained by the pipeline. Thus, we manually re-measured the redshift by using both emission lines and absorption lines. The emission lines of Hα λ6563, Hβ λ4861, [OII] λ3727, [OIII] $\lambda\lambda$4959,5007, [NII] $\lambda\lambda$6548, 6583 and [SII] $\lambda\lambda$6716,6731 and absorption lines of Ca HK (3933 Å, 3969 Å), Mg b line (5172 Å), NaI (5893 Å) and Hα (6563 Å) were adopted to determine the redshifts. The uncertainty in redshift by using this method was less than 0.001.

Finally, we obtained a sample of 1528 galaxies with effective redshift in Field A, which is twice the number derived from the pipeline. The redshift range is from 0.005 to 1.6. In Field A, 99% (1514/1528) of galaxies in our sample have $z < 0.3$. This is important for our morphological classifications in the following study.

2.2 WISE Data

The WISE all-sky survey contains hundreds of millions of objects at 3.4–22 µm (Wright et al. 2010; Yan et al. 2013). The AllWISE program is an extended project based on WISE, which combines both cryogenic and post-cryogenic survey data and covers the entire sky from January 2010 to February

Table 1 Morphology Classification of LIRGs

Galaxy Type	$\log(L_{\mathrm{TIR}}/L_\odot) \leqslant 11.3$	$11.3 < \log(L_{\mathrm{TIR}}/L_\odot) \leqslant 11.6$	$\log(L_{\mathrm{TIR}}/L_\odot) > 11.6$	Total
Spiral	25	5	1	31
Peculiar	15	4	2	21
Compact	9	1	2	12
Total	49	10	5	64

2011 (Klein et al. 2014). The AllWISE program reproduces a new source catalog and image atlas with enhanced sensitivity and accuracy compared with earlier WISE data releases.

2.3 Sample Selection

The sample galaxies in Field A are first cross-identified with the AllWISE catalog within a radius of $3''$. This process derives 1514/1528 objects that have infrared counterparts. In order to get reliable infrared luminosities, we only consider the sample galaxies with SNR >3 in 22 μm and $z < 0.3$. After the selection criteria are applied, only 316 galaxies remain.

To obtain the 22 μm (W4) luminosities at rest-frame, we have done the K-correction for all 316 galaxies by using Assef et al. (2010)'s fitting code with a series of spectral energy distribution (SED) templates. The templates include a galaxy with a pure old stellar population, a galaxy with continuous star-forming activity, a starburst galaxy and an AGN in the wavelength range from 0.03–30 μm. The code can derive the K-corrected magnitudes of all input filters simultaneously. In this paper, the five Petrosian magnitudes of SDSS $ugriz$ and four point-source profile-fitting magnitudes of WISE are adopted during the K-correction.

As we lack far-infrared flux, we need to use 22 μm monochromatic infrared luminosity to calculate the total infrared luminosity. Fortunately, many authors have investigated such a conversion factor to transform the mid-infrared luminosities to the total infrared luminosities (e.g. Dale & Helou 2002; Rieke et al. 2009; Boquien et al. 2010; Galametz et al. 2013).

As presented by Wen et al. (2014), the total flux conversion factor of the WISE 22 μm band is comparable to *Spitzer* 24 μm. Since the results of Galametz et al. (2013) are based on nearby galaxies, we should to test the feasibility of this method before performing our calculations. We obtain the sample from Cao et al. (2006), which is a sample of LIRGs selected from IRAS observations. We calculate their total luminosity by using the WISE 22 μm band under Galametz et al. (2013)'s conversion factor and compare to the result of Cao et al. (2006). We find that the total infrared luminosity still follows a linear relation between IRAS and the method of Galametz et al. (2013).

Therefore, we adopt the conversion factor of Galametz et al. (2013) in this work, which is shown as follows

$$\log L_{\mathrm{TIR}} = 0.954 \log \nu L_\nu (24\,\mu\mathrm{m}) + 1.336\,. \tag{1}$$

The combination forms the stack of spectra. Since all objects at least have three observations, we stacked them, after all removals.

Finally, we find 64 newly discovered LIRGs ($L_{\mathrm{TIR}} > 10^{11}\,L_\odot$) including one ULIRG ($L_{\mathrm{TIR}} > 10^{12}\,L_\odot$). The infrared luminosity distribution of all targets is presented in Figure 2. Among them, only five galaxies have spectral observations in SDSS DR 10 which means 59 galaxies are new spectral observations by LAMOST. Thus, the number density of LIRGs is about 3 objects deg^{-2}.
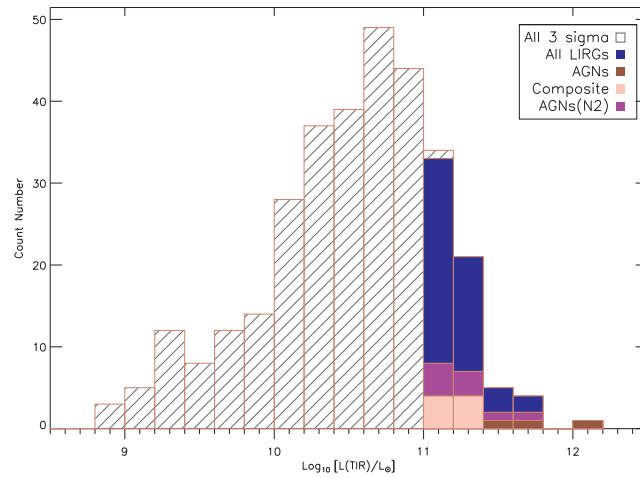
Fig. 2 The infrared luminosity distribution of all 3σ galaxies, all LIRG candidates and LIRGs with central AGNs in Field A. The luminosity cutoff is $L_{\mathrm{TIR}} > 10^{11} \ L_{\odot}$. Symbols are discussed in the following sections. The distribution reveals that the fraction of AGNs increases as the IR luminosity increases.
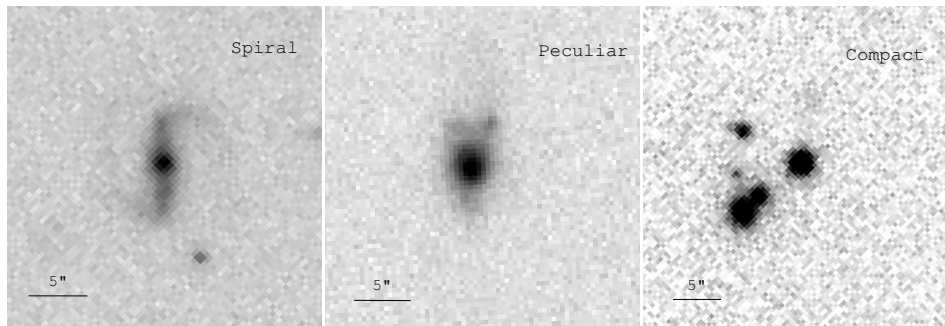

Fig. 3 The r-band images of sample galaxies with different morphological types. The names of our example galaxies are SDSS J022803.79+034507.8, SDSS J023933.69+033300.2 and SDSS J023527.75+042530.6 from left to right respectively.

3 RESULTS AND ANALYSES

3.1 Morphological Classifications

The morphological classification of galaxies in the sample is based on visual inspection by using the criterion of the Third Reference Catalogue of bright galaxies (RC3; de Vaucouleurs et al. 1991), which classifies the morphological types of galaxies according to the bulge ratio, spiral arm and interaction features. Our sample of LIRGs is divided into three different morphological types of spiral galaxies, peculiar galaxies and compact galaxies based on SDSS r-band images (see Fig. 3). The peculiar galaxies are determined by their asymmetric morphologies. The visual classification is performed by two of the authors, and their decisions are almost consistent.
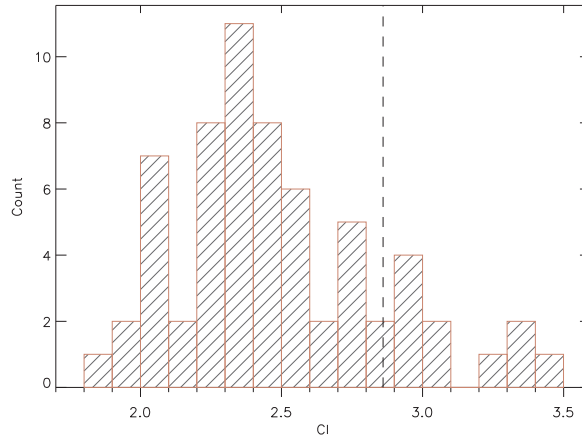
Fig. 4 The distribution of concentration index C for all LIRG candidates in Field A. This demonstrates that our selected galaxies are biased towards late-type galaxies.

In this sample, 48.4% (31/64) of the sample galaxies are classified as spiral galaxies, 32.8% (21/64) are classified as peculiar galaxies, and the other 18.8% (12/64) are classified as compact galaxies (see Table 1). The fraction of peculiar/compact galaxies in our sample is about 50%, which is similar to the morphological type fractions of Wang et al. (2006) (60%). This may indicate that our sample is consistent with the sample of Wang et al. (2006).

The concentration index is a quantitative parameter used to infer morphological types of galaxies (e.g. Shimasaku et al. 2001; Nakamura et al. 2003; Deng et al. 2012). It is computed by the ratio of galactic fluxes at two fixed radii which is a relative parameter that is not affected by external factors. We adopt the concentration index $C = R90/R50 < 2.86$ as the criterion for late-type galaxies and the others are classified as early-type galaxies.

Figure 4 shows the C distribution of our selected galaxies. In our sample, there are 53 galaxies with a low concentration index (C<2.86), which is consistent with the results of our visual classification.

3.2 Spectral Type Classification

Spectral classification is done by using both the BPT diagram ([NII]/Hα and [OIII]/Hβ) and flux criteria ([NII]/Hα) (Baldwin et al. 1981; Veilleux & Osterbrock 1987), since low SNR of blue channel spectra and the large uncertainty in the flux calibration of LAMOST spectra limit our ability to classify spectral type.

We first inspect the possible broad-line component by using multiple Gaussian spectral fittings of their spectral lines. Those galaxies with broad Hα emission lines are directly classified as AGNs, among which six galaxies are directly identified as broad-line AGNs.

Then, to assort the spectral type of the other targets, we first use the BPT diagram by applying multiple Gaussian spectral fittings to their spectral lines. The resulting locations on the BPT diagram are shown in Figure 5. The lower line and upper line are from Kauffmann et al. (2003) and Kewley et al. (2001), which are classified as star-forming galaxies and AGNs, respectively. Those galaxies between the two lines, which represent galaxies containing both star-forming galaxies and AGNs, are classified as composite galaxies. In our LAMOST sample, only 19 galaxies are detected with all four emission lines; 3 (15%) of them are classified as non-broad-line AGNs and 8 (40%) are
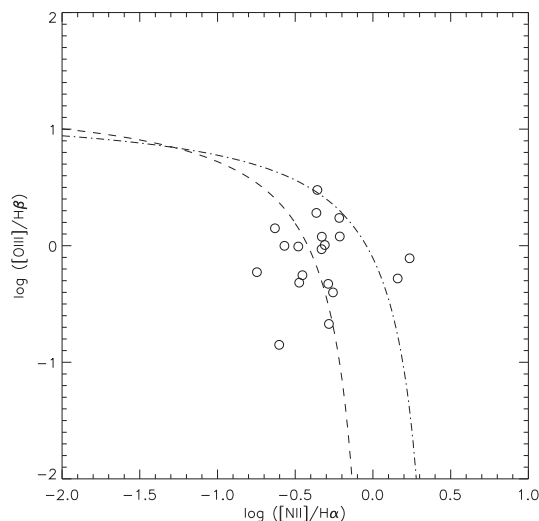
Fig. 5 The BPT diagram of our sample galaxies.

classified as composite galaxies. Thus, 11 galaxies with an AGN are classified by using the BPT diagram.

As we mentioned previously, the low SNR of the blue channel and large uncertainty in flux calibration affect our spectral type identification. Therefore, we also adopt the flux ratio of [NII]/Hα > 0.6 as a criterion to separate the narrow line AGNs from HII galaxies (Veilleux & Osterbrock 1987) for non-broad-line targets. Using this criterion, part of the composite galaxies between Kewley's line (Kewley et al. 2001) and Kauffmann's line (Kauffmann et al. 2003) may be classified as AGNs. The total number of AGNs (except the galaxies in the BPT diagram) identified using this method are 11.
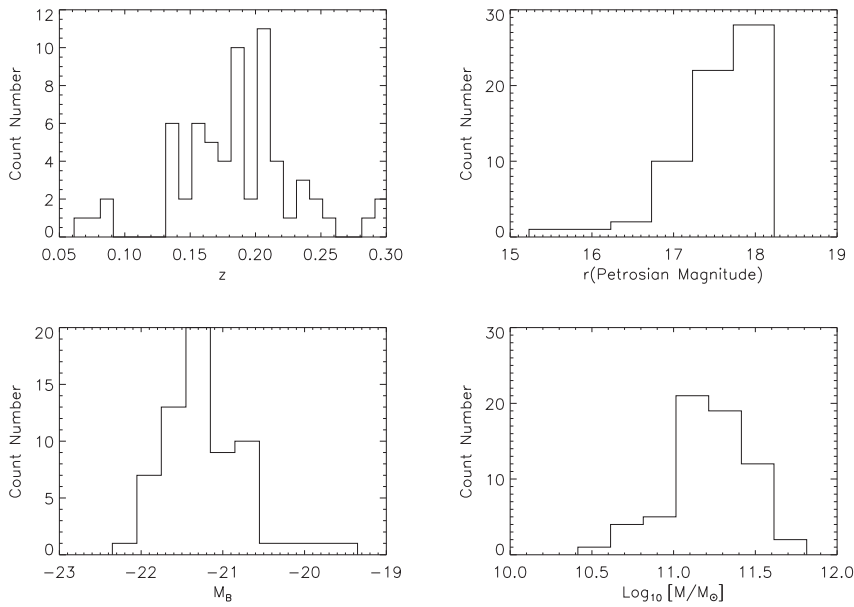
3.3 Sample Distributions

The distributions of redshift, Petrosian r magnitude, stellar mass and B-band absolute magnitude are shown in Figure 6. The redshifts of sample galaxies are from 0.05 to 0.30. The magnitude is cut-off at $r = 18.1$ mag, and the bright end of magnitude is $r = 15.2$ mag. The stellar masses of our sample LIRGs have a narrow range from $10^{10.4}$ to $10^{11.8} M_\odot$, with a peak of $10^{11} M_\odot$, which is similar to the result of Wang et al. (2006) (further details are in Sect. 3.3). The B-band absolute magnitude (M_B) spans a wide range from –19.5 to –22.5 mag. The M_B is calculated from the SDSS g- and r-band magnitudes by using the relation between SDSS magnitude and $UBVRcIc$ magnitude given by Lupton (2005)[1]. The systematic error of this relation is 0.011 mag.

3.4 Colors

The WISE mid-infrared color-color diagrams are shown in Figure 7. As presented by Jarrett et al. (2011), the W1 and W2 bands are sensitive to the old stellar population and hot dust, the W3 band is sensitive to PAH emission, and the W4 band is contributed by very small dust grains (VSGs). W3 and W4 are dominated by dust which is heated by young stars or obscured AGNs. Therefore, the color-color diagrams can be used to classify the galaxies into types.

---

[1] *https://www.sdss3.org/dr10/algorithms/sdssUBVRITransform.php#Lupton2005*

Fig. 6 Distributions of sample galaxies. (a) redshift; (b) SDSS r-band Petrosian magnitude; (c) B-band absolute magnitude; (d) stellar mass.
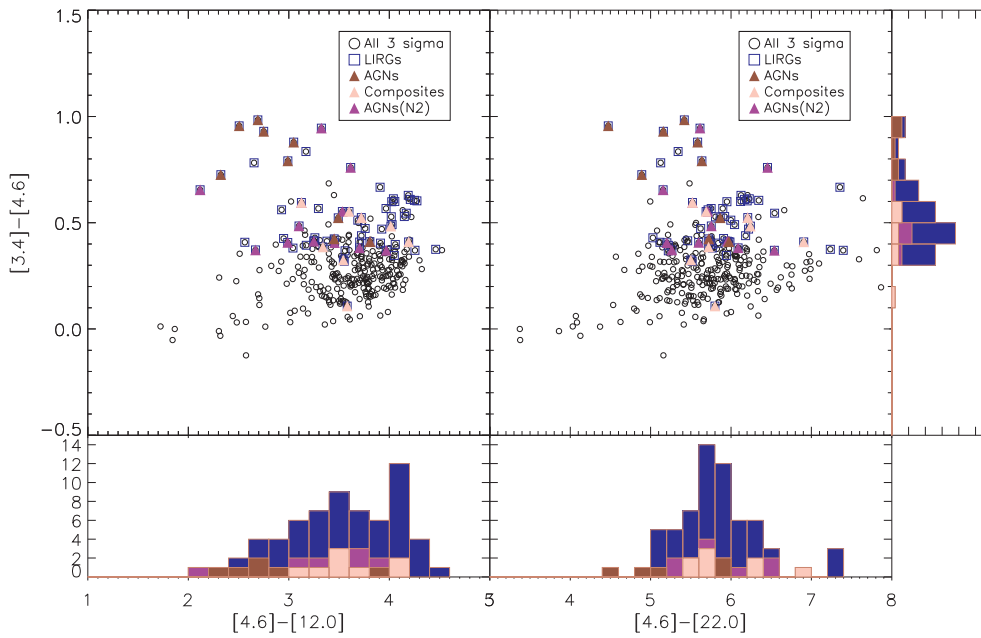
Fig. 7 The color-color diagrams of all 22 μm 3σ sample galaxies, LIRGs and LIRGs with central AGNs. The selected LIRGs reside in regions with obscured AGNs/AGNs, starbursts and LIRGs in figure 26 of Jarrett et al. (2011).

Compared with figure 26 of Jarrett et al. (2011), the selected LIRGs reside in the regions of AGNs, starburst and LIRGs identified in that article. As shown in Figure 7, the color of [3.4]–[4.6] indeed separates the AGNs from other cases. This supports Jarrett et al. (2011)'s result that most galaxies with [3.4]–[4.6] > 0.8 are AGNs. However, from our figure, the color value of [3.4]–[4.6] >0.7 could be a better boundary between AGNs and other cases. Two galaxies with [3.4]–[4.6] >0.7, which are not classified as AGNs in our optical spectra, may be dust obscured AGNs. The difference in mid-infrared colors of LIRGs indicates that the spectral energy distributions (SEDs) of LIRGs that are dominated by AGNs compared to LIRGs that are dominated by starbursts are quite different in the mid-infrared range.

As Wu et al. (2007) point out, strong AGNs could destroy the dust, especially PAHs (e.g. WISE 12 μm band), and elevate the VSG continuum in the mid-infrared band (e.g. both 12 and 22 μm). From Figure 7, the trend in colors shows that strong AGNs prefer to have lower values of both [4.6]–[12] and [4.6]–[22] colors and higher values of [3.4]–[4.6] colors, which is consistent with the result of Wu et al. (2007).

3.5 Star Formation Rate, Stellar Mass and Specific Star Formation Rate

The left panels of Figure 8 show the distributions of infrared luminosity for different morphological types. Except for a ULIRG, the infrared luminosities of spiral LIRGs are all less than $10^{11.5} L_\odot$. In fact, the sole ULIRG is not a normal spiral. Based on its spectra and [3.4]–[4.6] color, it is an IR-QSO which could be in the late phase of a merger (see Sect. 4.1). Compared with spiral LIRGs, parts of the peculiar/compact LIRGs could have higher infrared luminosity than $10^{11.5} L_\odot$. All these support the results of Wang et al. (2006) and Ishida (2004). The relation between merger fraction and infrared luminosity reveals that intensive star formation induced by a galactic merger is an important mechanism to explain the higher infrared luminosity phase ((U)LIRGs) of galaxies (e.g. Veilleux et al. 2002; Ishida 2004; Ellison et al. 2013).

The star formation rate (SFR) of LIRGs is derived following the result of Cluver et al. (2014)

$$\log \mathrm{SFR}(M_\odot \, \mathrm{yr}^{-1}) = 0.82 \log \nu L_{22 \, \mu\mathrm{m}} - 7.3 \,. \tag{2}$$

Here, the Chabrier initial mass function (IMF) is adopted. To transform the Chabrier-IMF to the Salpeter-IMF (Kennicutt 1998), a factor of 0.66 needs to be applied (Rieke et al. 2009).

The stellar mass is another important parameter associated with galaxies which is calculated from SDSS photometric data by using Bell et al. (2003)

$$\log(M_\star/M_\odot) = -0.4(M_{r,\mathrm{AB}} - 4.67) + [a_r + b_r(g - r)_{\mathrm{AB}} + 0.15] \,, \tag{3}$$

where $M_{r,\mathrm{AB}}$ is the r-band absolute magnitude and $(g - r)_{\mathrm{AB}}$ is the rest-frame color in AB magnitude. The coefficients a_r and b_r are taken from Bell et al. (2003). Based on the assumption of a Salpeter-IMF, the stellar masses of our sample are consistent with Wang et al. (2006), being only 0.1 dex higher. Moreover, we calculate the stellar masses of our sample by using Wen et al. (2013) based on the Kroupa-IMF, and find no significant deviation between Bell et al. (2003) and Wen et al. (2013), even if the IMFs used by the two methods are different. The middle column in Figure 8 shows the stellar mass distribution for different morphologies of LIRGs. The median stellar masses of peculiar and compact galaxies are almost the same, but the median value of spiral galaxies is slightly higher by about 0.2 dex. This indicates that normal star formation in a massive disk can produce similar infrared luminosity as that in intensive nuclear star formation. However, it is difficult for the infrared luminosity of a massive disk to exceed $10^{11.5} L_\odot$, as pointed out above.

The specific star formation rate (sSFR) is defined as the ratio of SFR to stellar mass. It is the parameter that expresses the intensity of star formation. The right column of Figure 8 gives the distribution of sSFRs. The median value of sSFR for spiral LIRGs is far lower than those of peculiar and compact LIRGs. Although there is similar infrared luminosity, star formation in spirals could spread
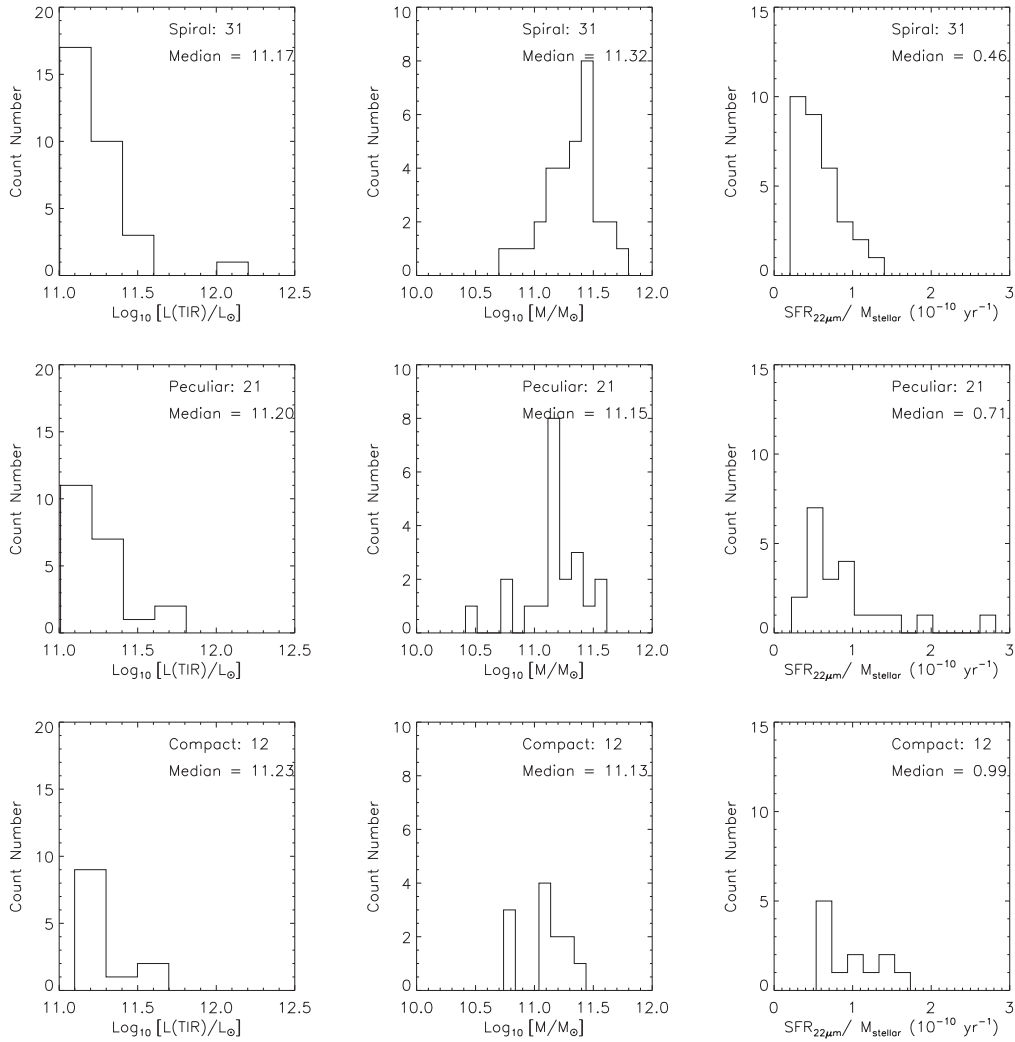
Fig. 8 The distributions of infrared luminosity and stellar mass of three morphological types of LIRGs. From top to bottom: spiral; peculiar; compact.

out all over the disk which leads to a lower intensity of star formation than nuclear starbursts. As expected, peculiar and compact LIRGs have higher values of sSFRs, which can be well explained by a merger-induced starburst. The sSFRs of LIRGs range from 0.02 to 0.27 Gyr^{-1}, which is consistent with the value in Pérez-González et al. (2005) of $z = 0 \sim 0.4$.

4 DISCUSSION

4.1 ULIRG: J023832.67+023349.1

SDSS J023832.67+023349.1 is the only ULIRG in our LIRG sample with $\log L(\mathrm{TIR}) = 12.08$. Although the morphologies of most low-z ULIRGs exhibit the feature of a merger or interaction

('Peculiar') (Wang et al. 2006; Ishida 2004), the morphology of SDSS J023832.67+023349.1 is a typical spiral without any significant interaction/merging feature in optical and near-infrared images. However, its mid-infrared color [3.4]–[4.6] is higher than 0.8 (Jarrett et al. 2011), which is the boundary to separate the AGNs. Also, its optical spectrum shows significant AGN features. Shi et al. (2014) reported that SDSS J023832.67+023349.1 has double-peaked narrow emission lines and could be fitted by two AGN components. Considering its high infrared luminosity, it may really be an IR-QSO candidate in the late stage of an interaction/merging event, rather than a normal spiral. Shi et al. (2014) classify this galaxy as an extended object, which is consistent with our classification. As a possible transitional object undergoing a merger, SDSS J023832.67+023349.1 is worth further investigations at different wavelengths.

4.2 Samples of LIRGs from WISE and IRAS

Until now, the sample of LIRGs has mainly been based on the IRAS survey, such as a sample of the most nearby cases from the Great Observatories All-Sky LIRG Survey (GOALS; Armus et al. 2009) and the largest sample matched by SDSS-DR2 and IRAS by Cao et al. (2006). Because of the observational limit of IRAS, the density of Cao et al. (2006)'s sample is only $\sim$0.64 deg^{-2} and the median redshift is around 0.1. However, the density of this work is $\sim$3 deg^{-2} and the median redshift is around 0.2. Moreover, observations using 12 μm from WISE are about two orders of magnitude more (Yan et al. 2013) sensitive than those of IRAS in the same band. Thus, there is an opportunity to obtain a large sample of LIRGs at higher redshift based on the WISE 22 μm catalog. In our work, only one ULIRG is found in 20 deg^2, and the density is around 0.05 deg^{-2}. Compared to previous studies of ULIRGs by Su et al. (2013) ($\sim$0.029 deg^{-2}) and Hou et al. (2009) ($\sim$0.04 deg^{-2}), the ULIRG density in our work is consistent with their results.

According to the redshift distribution of LIRGs in this paper, we expect to construct the largest samples of LIRGs at redshift of 0.2 with the spectroscopic redshifts of LAMOST and SDSS. Based on the number density estimated here, it would include more than ten thousand LIRGs and be very helpful for studying the properties and possible evolution of LIRGs in the future.

5 SUMMARY

In this paper, we construct a sample of LIRGs based on cross-identification between the AllWISE survey catalog and one field of the LAMOST (Guo Shou Jing Telescope) LCSSPA at SGC, and obtain the following results:

(1) A total of 64 new LIRGs are obtained in the 20 deg^2 of Field A from LCSSPA, and the number density of LIRGs is $\sim$3 deg^{-2}.
(2) The fraction of morphological types in our sample is Spiral: Peculiar: Compact = 48.4%: 32.8%: 18.8%. Though more than 40% of our targets are disk galaxies, the peculiar and compact galaxies still show higher infrared luminosities.
(3) The mid-infrared color of [3.4]–[4.6] can be used to distinguish AGNs from other cases.
(4) The sole ULIRG, SDSS J023832.67+023349.1, is an IR-QSO in the late phase of a merger.

The Guo Shou Jing Telescope (the Large Sky Area Multi-Object Fiber Spectroscopic Telescope, LAMOST) is a National Major Scientific Project built by Chinese Academy of Sciences. Funding for the project has been provided by the National Development and Reform Commission. LAMOST is operated and managed by National Astronomical Observatories, Chinese Academy of Sciences.

This publication makes use of data products from the Wide-field Infrared Survey Explorer, which is a joint project of the University of California, Los Angeles, and the Jet Propulsion Laboratory/California Institute of Technology, and is funded the National Aeronautics and Space Administration.

Appendix A: THE CATALOG OF LIRGS

Table A.1 Catalog of LIRGs

RA (hh:mm:ss)	Dec (hh:mm:ss)	redshift(z)	Petrosian r (mag)	kc (22 µm) (mag)	L (TIR) ($\log L_\odot$)	Morphology	Spectral Type
(1)	(2)	(3)	(4)	(5)	(6)	(7)	(8)
02:31:13.46	01:06:59	0.1815	17.65	−0.16	11.11	Compact	Star-forming
02:24:20.65	01:58:41	0.1516	16.43	−0.14	11.43	Spiral	AGN(N2)
02:33:28.46	02:48:00	0.1716	17.84	−0.15	11.20	Peculiar	AGN(N2)
02:27:23.16	01:24:07	0.1515	16.92	−0.13	11.39	Spiral	Unknown
02:28:22.09	02:15:12	0.1405	16.94	−0.14	11.18	Spiral	AGN
02:23:26.51	02:42:32	0.1835	18.00	−0.15	11.24	Peculiar	Unknown
02:23:41.64	03:40:31	0.1428	16.95	−0.14	11.04	Spiral	Unknown
02:33:48.39	04:18:16	0.1675	17.66	−0.12	11.37	Compact	Star-forming
02:26:09.58	03:22:48	0.2225	18.00	−0.17	11.02	Spiral	Star-forming
02:26:54.48	03:58:13	0.2069	17.95	−0.08	11.13	Peculiar	Unknown
02:24:39.34	05:08:50	0.1927	17.50	−0.16	11.21	Compact	Unknown
02:27:50.85	01:15:15	0.1863	17.60	−0.12	11.37	Peculiar	Unknown
02:28:51.73	01:57:47	0.1888	17.94	−0.16	11.23	Compact	Unknown
02:29:19.08	02:31:22	0.1403	17.21	−0.14	11.01	Peculiar	Star-forming
02:29:43.78	03:12:47	0.2059	17.65	−0.15	11.02	Spiral	AGN(N2)
02:30:03.78	03:24:28	0.1585	17.82	−0.13	11.12	Peculiar	Unknown
02:33:36.86	03:41:57	0.2026	17.90	−0.09	11.03	Spiral	AGN(N2)
02:28:34.66	04:17:21	0.2101	17.88	−0.17	11.01	Peculiar	Broad-line
02:29:55.94	04:04:52	0.1841	18.04	−0.16	11.17	Peculiar	Unknown
02:31:21.82	05:14:44	0.2337	18.07	−0.16	11.06	Spiral	Broad-line
02:29:50.12	04:19:42	0.211	18.00	−0.16	11.11	Compact	AGN(N2)
02:22:57.52	02:27:09	0.1778	17.89	−0.15	11.68	Peculiar	Unknown
02:22:35.02	02:36:50	0.2071	17.93	−0.15	11.22	Spiral	AGN(N2)
02:34:46.90	01:40:47	0.1867	17.88	−0.13	11.17	Spiral	Unknown
02:30:35.23	01:57:36	0.2438	18.00	−0.17	11.31	Peculiar	Unknown
02:32:54.18	01:16:21	0.2528	18.05	−0.09	11.41	Peculiar	Composite
02:25:33.83	04:02:16	0.1863	18.05	−0.16	11.14	Compact	Star-forming
02:30:00.46	05:06:00	0.1543	16.96	−0.14	11.11	Spiral	AGN(N2)
02:22:56.75	02:24:16	0.178	17.59	−0.16	11.28	Spiral	Unknown
02:27:47.58	03:34:36	0.1888	17.48	−0.15	11.25	Peculiar	Unknown
02:28:03.79	03:45:07	0.1909	17.34	−0.11	11.59	Spiral	Unknown
02:21:55.82	04:05:28	0.0855	17.38	−0.09	11.01	Spiral	AGN(N2)
02:29:29.57	02:51:38	0.234	18.07	−0.14	11.78	Peculiar	Unknown
02:34:07.98	05:34:46	0.1391	17.94	−0.14	11.17	Compact	Composite

Table A.1 — *Continued.*

RA (hh:mm:ss) (1)	Dec (hh:mm:ss) (2)	redshift (z) (3)	Petrosian r (mag) (4)	kc (22 μm) (mag) (5)	L (TIR) (log $L_\odot$) (6)	Morphology (7)	Spectral Type (8)
02:22:29.54	02:36:35	0.2074	17.93	–0.16	11.24	Spiral	AGN
02:26:49.98	01:35:35	0.205	17.97	–0.16	11.26	Peculiar	Unknown
02:22:50.79	02:52:44	0.2141	17.93	–0.17	11.25	Spiral	Composite
02:28:12.94	04:43:32	0.2121	17.71	–0.16	11.60	Compact	Unknown
02:34:09.61	04:42:57	0.2824	18.03	–0.22	11.36	Spiral	Composite
02:34:47.39	04:44:42	0.1379	17.80	–0.14	11.26	Spiral	Unknown
02:35:05.59	03:03:12	0.2036	17.47	–0.16	11.46	Peculiar	Unknown
02:32:47.10	04:59:02	0.1831	18.02	–0.15	11.28	Spiral	Broad-line
02:24:01.22	03:41:19	0.1917	17.35	–0.16	11.23	Spiral	Broad-line
02:32:12.53	02:19:03	0.2432	17.95	–0.19	11.17	Spiral	Composite
02:32:42.06	01:23:53	0.1606	17.81	–0.15	11.02	Spiral	Unknown
02:24:08.82	03:32:42	0.142	16.99	–0.14	11.06	Peculiar	Unknown
02:22:42.33	03:38:20	0.2163	18.06	–0.17	11.22	Spiral	AGN(N2)
02:37:20.30	05:04:48	0.1595	17.87	–0.15	11.10	Compact	Unknown
02:29:15.75	03:24:35	0.0794	15.29	–0.08	11.03	Spiral	Broad-line
02:35:40.36	02:34:09	0.1638	17.74	–0.15	11.26	Compact	Star-forming
02:37:01.79	02:40:22	0.0875	16.01	–0.14	11.24	Peculiar	Composite
02:38:32.67	02:33:49	0.2082	17.09	–0.08	12.08	Spiral	AGN
02:35:35.92	03:06:32	0.1394	17.70	–0.14	11.15	Peculiar	Unknown
02:37:33.67	02:56:24	0.2075	17.81	–0.18	11.08	Spiral	Unknown
02:36:48.77	03:05:20	0.2343	17.55	–0.18	11.16	Peculiar	Composite
02:39:12.54	03:30:31	0.1667	16.88	–0.15	11.11	Spiral	Unknown
02:39:33.69	03:33:00	0.1396	17.39	–0.14	11.08	Peculiar	AGN(N2)
02:36:44.23	04:07:48	0.1719	17.88	–0.15	11.25	Compact	Broad-line
02:38:48.14	04:02:08	0.1711	17.44	–0.15	11.06	Spiral	AGN(N2)
02:39:27.23	03:42:44	0.1665	17.84	–0.15	11.00	Spiral	Unknown
02:35:46.85	04:10:40	0.2939	18.02	–0.18	11.47	Spiral	Composite
02:38:47.62	04:19:17	0.217	17.96	–0.07	11.15	Spiral	Star-forming
02:40:53.31	04:11:22	0.0613	16.69	–0.07	11.02	Peculiar	Unknown
02:35:27.75	04:25:30	0.299	17.99	–0.008	11.61	Compact	Star-forming

References

Armus, L., Mazzarella, J. M., Evans, A. S., et al. 2009, PASP, 121, 559

Assef, R. J., Kochanek, C. S., Brodwin, M., et al. 2010, ApJ, 713, 970

Baldwin, J. A., Phillips, M. M., & Terlevich, R. 1981, PASP, 93, 5

Bell, E. F., McIntosh, D. H., Katz, N., & Weinberg, M. D. 2003, ApJS, 149, 289

Boquien, M., Bendo, G., Calzetti, D., et al. 2010, ApJ, 713, 626

Cao, C., Wu, H., Wang, J.-L., et al. 2006, ChJAA (Chin. J. Astron. Astrophys.), 6, 197

Cluver, M. E., Jarrett, T. H., Hopkins, A. M., et al. 2014, ApJ, 782, 90

Cui, X.-Q., Zhao, Y.-H., Chu, Y.-Q., et al. 2012, RAA (Research in Astronomy and Astrophysics), 12, 1197

Dale, D. A., & Helou, G. 2002, ApJ, 576, 159

de Vaucouleurs, G., de Vaucouleurs, A., Corwin, Jr., H. G., et al. 1991, Third Reference Catalogue of Bright
 Galaxies (New York: Springer), 2091

Deng, X.-F., Wu, P., Qian, X.-X., & Luo, C.-H. 2012, PASJ, 64, 93

Eisenhardt, P. R. M., Wu, J., Tsai, C.-W., et al. 2012, ApJ, 755, 173

Ellison, S. L., Mendel, J. T., Scudder, J. M., Patton, D. R., & Palmer, M. J. D. 2013, MNRAS, 430, 3128

Galametz, M., Kennicutt, R. C., Calzetti, D., et al. 2013, MNRAS, 431, 1956

Hung, C.-L., et al., 2014, ApJ, 791, 63

Hou, L. G., Wu, X.-B., & Han, J. L. 2009, ApJ, 704, 789

Ishida, C. M. 2004, PhD Thesis (University of Hawai'i)

Jarrett, T. H., Cohen, M., Masci, F., et al. 2011, ApJ, 735, 112

Kauffmann, G., Heckman, T. M., Tremonti, C., et al. 2003, MNRAS, 346, 1055

Kennicutt, Jr., R. C. 1998, ARA&A, 36, 189

Kewley, L. J., Heisler, C. A., Dopita, M. A., & Lumsden, S. 2001, ApJS, 132, 37

Klein, C. R., Richards, J. W., Butler, N. R., & Bloom, J. S. 2014, MNRAS, 440, L96

Liu, X. W., Zhao, G., & Hou, J. L. 2015, RAA (Research in Astronomy and Astrophysics), 15, 1089

Luo, A.-L., Zhang, H.-T., Zhao, Y.-H., et al. 2012, RAA (Research in Astronomy and Astrophysics), 12, 1243

Melbourne, J., Koo, D. C., & Le Floc'h, E. 2005, ApJ, 632, L65

Nakamura, O., Fukugita, M., Yasuda, N., et al. 2003, AJ, 125, 1682

Neugebauer, G., Soifer, B. T., Beichman, C. A., et al. 1984, Science, 224, 14

Pérez-González, P. G., Rieke, G. H., Egami, E., et al. 2005, ApJ, 630, 82

Rieke, G. H., Alonso-Herrero, A., Weiner, B. J., et al. 2009, ApJ, 692, 556

Sanders, D. B., & Mirabel, I. F. 1996, ARA&A, 34, 749

Shi, Zhi-Xin, et al., 2014, RAA (Research in Astronomy and Astrophysics), 14, 1234

Shimasaku, K., Fukugita, M., Doi, M., et al. 2001, AJ, 122, 1238

Soifer, B. T., Neugebauer, G., & Houck, J. R. 1987, ARA&A, 25, 187

Su, S., Kong, X., Li, J., & Fang, G. 2013, ApJ, 778, 10

Surace, J. A., Sanders, D. B., Vacca, W. D., Veilleux, S., & Mazzarella, J. M. 1998, ApJ, 492, 116

Veilleux, S., & Osterbrock, D. E. 1987, ApJS, 63, 295

Veilleux, S., Kim, D.-C., & Sanders, D. B. 2002, ApJS, 143, 315

Wang, J.-L. 2008, ChJAA (Chin. J. Astron. Astrophys.), 8, 643

Wang, J. L., Xia, X. Y., Mao, S., et al. 2006, ApJ, 649, 722

Wen, X.-Q., Wu, H., Zhu, Y.-N., et al. 2013, MNRAS, 433, 2946

Wen, X.-Q., Wu, H., Zhu, Y.-N., et al. 2014, MNRAS, 438, 97

Wright, E. L., Eisenhardt, P. R. M., Mainzer, A. K., et al. 2010, AJ, 140, 1868

Wu, H., Zou, Z. L., Xia, X. Y., & Deng, Z. G. 1998a, A&AS, 127, 521

Wu, H., Zou, Z. L., Xia, X. Y., & Deng, Z. G. 1998b, A&AS, 132, 181

Wu, H., Zhu, Y.-N., Cao, C., & Qin, B. 2007, ApJ, 668, 87

Yan, L., Donoso, E., Tsai, C.-W., et al. 2013, AJ, 145, 55

Zhao, G., Zhao, Y.-H., Chu, Y.-Q., Jing, Y.-P., & Deng, L.-C. 2012, RAA (Research in Astronomy and Astrophysics), 12, 723

Zou, Z., Xia, X., Deng, Z., & Su, H. 1991, MNRAS, 252, 593